



## Full Text View

[Volume 29, Issue 10 \(October 1999\)](#)

## Journal of Physical Oceanography

Article: pp. 2541–2558 | [Abstract](#) | [PDF \(1.16M\)](#)

# Mean Structure and Interannual Variability of the Slopewater System South of Newfoundland\*

Robert S. Pickart, Theresa K. McKee, Daniel J. Torres, and Stephanie A. Harrington

*Woods Hole Oceanographic Institution, Woods Hole, Massachusetts*

(Manuscript received December 30, 1997, in final form November 12, 1998)

DOI: 10.1175/1520-0485(1999)029<2541:MSAIVO>2.0.CO;2

## ABSTRACT

Two sets of repeat hydrographic sections, centered at 55°W and 50°W, are used to study the mean features and long-term variability of the slopewater system south of Newfoundland, inshore of the Gulf Stream. The upper-layer flow is considered first, consisting of the westward-flowing Labrador Current at the shelfbreak (input into the slopewater system) and the eastward-flowing slopewater current over midslope (export out of the slopewater system). Particular attention is paid to the slopewater current, as this is a less well-known feature. The velocity structure of the slopewater current is different at the two longitudes, associated with a change in structure of the density front. Its mean transport is found to be significantly less than historical estimates. Both the lateral position and the strength of the current vary on long timescales. These fluctuations are correlated with the variability of the Labrador Current, as well as with changes in the deeper components of the slopewater (the Labrador Sea Water and Denmark Strait overflow water). The general picture that emerges is that the entire upper-layer slopewater circulation spins up/down on interannual timescales, coincident with strengthening/weakening of the overflow component of the deep western boundary current. Interestingly, more undiluted Labrador Sea Water is present in the spundown state.

## 1. Introduction

In a recent study, [Pickart and Smethie \(1998\)](#), hereafter PS) investigated the temporal variability of the deep western boundary current (DWBC) at 55°W, south of the island of Newfoundland. Their work focused on the deep flow and addressed the major water masses of the DWBC, which varied significantly over a 12-yr period. The argument was made that repeat hydrography collected in the

## Table of Contents:

- [Introduction](#)
- [Slopewater circulation](#)
- [Approach](#)
- [Upper-layer flow at 55°W:](#)
- [Upper-layer flow at 50°W:](#)
- [Coupled shallow–deep](#)
- [Conclusions](#)
- [REFERENCES](#)
- [TABLES](#)
- [FIGURES](#)

## Options:

- [Create Reference](#)
- [Email this Article](#)
- [Add to MyArchive](#)
- [Search AMS Glossary](#)

## Search CrossRef for:


- [Articles Citing This Article](#)

## Search Google Scholar for:

- [Robert S. Pickart](#)
- [Theresa K. McKee](#)
- [Daniel J. Torres](#)
- [Stephanie A. Harrington](#)


DWBC should be particularly revealing, since climate anomalies originating from the northern deep-water formation sites should appear in the DWBC first. Indeed it has been demonstrated that the western boundary plays an important role in the climate system (e.g., [Curry et al. 1998](#)). However, the robust circulation at the boundary also results in enhanced local variability, which in fact can make the task of identifying true climate signals more challenging.


In this paper we expand on the analysis of PS and consider the entire water column, using a more extensive historical dataset. We focus again on the slopewater region south of Newfoundland, which is an important area where waters of subtropical and subpolar origin meet and interact. Our intention is to use enough data to compute robust mean fields and extract unambiguously the dominant interannual signals. In doing so we demonstrate the difficulty (and danger) of using small numbers of repeat observations to deduce conclusions regarding climate change. More interestingly, we shed light on the mean structure of the upper slopewater circulation and reveal an intriguing coupling of the long-term variability that involves both the shallow and deep components of the slopewater system.


Our presentation begins with a brief overview of the circulation and water mass structure inshore of the Gulf Stream south of Newfoundland. Despite numerous measurement programs through the years, there are basic aspects of the slopewater system that are not very well understood. The historical data used in the present study are then described. We consider two sets of near-repeat hydrographic sections: one set centered at 55°W, the second set located at 50°W ([Fig. 1](#) ). Our analysis focuses first on the upper-layer circulation, in particular on the eastward-flowing slopewater current, which resides over midslope, and the westward-flowing Labrador Current located at the shelfbreak. Both the mean state as well as interannual fluctuations of the upper-layer flow are considered; our analysis provides the most quantitative view to date of the slopewater current. We then investigate the coupled nature of the variability throughout the water column, which raises some important implications.

## 2. Slopewater circulation south of Newfoundland: A brief historical overview

### *a. Upper layer*

The circulation near the Grand Banks of Newfoundland is remarkably complex, consisting of a series of thermohaline and wind-driven currents extending from the shelfbreak to the deep slope ([Fig. 2](#) ). In the upper layer the Gulf Stream flows eastward, usually located near 39°N (Fuglister 1963), before bifurcating: the southern portion branches to the southeast while the remaining flow progresses past the Grand Banks and turns northward as the North Atlantic Current. Near the shelfbreak the main branch of the Labrador Current flows equatorward, carrying cold, fresh water of subpolar and arctic origins ([Lazier and Wright 1993](#)). In the vicinity of the Grand Banks a portion of the Labrador Current retroflects back to the east inshore of the North Atlantic Current ([Clarke et al. 1980](#)). It is unknown what percentage of the jet actually retroflects, but some of the transport clearly continues equatorward ([McLellan 1957](#); [Petrie and Drinkwater 1993](#); [Loder et al. 1998](#)).

Between the shelfbreak and the Gulf Stream there is a separate eastward current at these longitudes known as the slopewater current (or jet), which is associated with a strong temperature and salinity front (upper layer, [Fig. 3a](#) ). Since the reader may not be familiar with this current, we offer a brief historical perspective. For many years the slopewater jet was confused with the Gulf Stream (or North Atlantic Current). This was partly due to the fact that the International Ice Patrol repeat hydrographic sections at 50°W did not extend far enough south to sample the Gulf Stream proper. Using data from a multiship experiment, [Fuglister and Worthington \(1951\)](#) clearly established that the slopewater current was indeed a separate entity from the Gulf Stream. This was further verified by [McLellan \(1957\)](#), who studied its water mass composition and gave the current its name.

[Fuglister and Worthington \(1951\)](#) hypothesized that the slopewater current extended all the way from Cape Hatteras to the Grand Banks, with a westward-flowing countercurrent between it and the Gulf Stream. However, hydrographic sections northeast of Cape Hatteras do not always detect the slopewater jet. The Gulf Stream '60 Experiment, which synoptically occupied sections from Cape Cod to the Grand Banks, showed the jet “splitting” off of the Gulf Stream south of Nova Scotia (see also [Fofonoff and Hall 1983](#)). Thus, the evidence suggests that, in the mean, the slopewater current bifurcates from the Gulf Stream somewhere around 60°W ([Fig. 2](#) ). This is to the east of the western slope–sea cyclonic gyre described by Csanady and Hamilton (1983). The occasional observations of a slopewater jet west of 60°W may, in fact, be the southern limb of the Csanady and Hamilton (1983) gyre, which otherwise seems to be adjacent to the Gulf Stream. (This, however, is speculation on our part.) Historical current meter measurements from the eastern slope region have not, in general, detected the slopewater current. This may be due to insufficient horizontal resolution (e.g., [Richardson 1985](#)) or lack of data in the upper portion of the water column (e.g., [Hendry 1993](#)). [Richardson's \(1985\)](#) mean geostrophic section at 55°W does show a distinct slopewater jet, though in that study it was treated as part of the Gulf Stream.

The precise fate of the slopewater current to the east remains an open issue. The most extensive experiment to date that might have shed light on this was the joint Canadian–U.S. hydrographic program in 1972 in the vicinity of the Grand Banks ([Clarke et al. 1980](#)). However, during that time period the Gulf Stream was far north of its normal latitude and “merged”

with the slopewater current, making it impossible to distinguish the two. During the more typical configuration depicted in [Fig. 2](#), the slopewater jet may join the retroflected portion of the Labrador Current and exit the region either inshore of, or as part of, the North Atlantic Current (e.g., [Mann 1967](#); [Mountain and Shuhly 1980](#); Csanady and Hamilton 1983). Worthington (1976) suggests that the slopewater current is instead the northern limb of a closed anticyclonic eastern slope gyre, with all of its transport turning back to the west near the Tail of the Grand Banks. While this scenario downplays the importance of the bifurcation seen in the Gulf Stream '60 data, it is consistent with measurements of westward counterflow just inshore of the Gulf Stream reported by [Fuglister and Worthington \(1951\)](#). [McLellan \(1957\)](#) points out, however, that such a countercurrent is the exception and not the rule.<sup>1</sup> Both descriptions could, in fact, hold true to some degree; this will require further measurements to sort out. Regardless of its exact origin and fate, however, the Slopewater Current is a permanent component of the circulation system south of Newfoundland and is a major feature in our two historical datasets.

### *b. Lower layer*

The vicinity of the Grand Banks is also a region of critical importance for the deep circulation. The major subthermocline current in the slopewater is the DWBC, transporting water of northern origin toward the equator. The main water mass constituents of the current are (progressing deep to shallow) the Denmark Strait overflow water (centered near 3500 m), classical Labrador Sea Water (1500 m), and upper Labrador Sea Water (800 m). [Pickart and Smethie \(1998\)](#) describe the deep-water mass structure in detail using a portion of the data used here. Their mean absolute geostrophic velocity section nicely illustrates the distribution of currents throughout the water column ([Fig. 3b](#)). One sees enhanced equatorward flow of both the overflow water banked against the slope near 3500 m and classical Labrador Sea Water near 1500 m. The slopewater jet is evident as the eastward flow in the upper layer located laterally near 140 km, precisely where the associated salinity front resides in [Fig. 3a](#) (note that the section ends north of the Gulf Stream).

As is true in the upper layer, basic questions exist regarding the fate of the deep flow as it encounters the tail of the Grand Banks. The Southeast Newfoundland Ridge diverts the DWBC offshore toward the North Atlantic Current. This may lead to an interaction of these two currents similar to that which occurs at Cape Hatteras, where a portion of the DWBC is entrained into the Gulf Stream ([Pickart and Smethie 1993](#)). The ridge itself may also act as a potential vorticity barrier, causing recirculation of the deep flow ([Pickart and Huang 1995](#)). In any event, the deepest portion of the DWBC apparently cannot negotiate the Southeast Newfoundland Ridge and either recirculates or becomes diverted into the subtropical Gulf Stream system. We are concerned here only with that portion of the DWBC that progresses past the Grand Banks along the continental slope.

## 3. Approach

In this study we analyze two sets of near-repeat hydrographic sections in the slopewater south of Newfoundland, addressing both the mean structure and interannual variability. The nominal longitude of the first set of sections is 55°W. [Pickart and Smethie \(1998\)](#) recently analyzed four “exact” repeats at this longitude collected between 1983 and 1995, focusing on the subthermocline water masses of the DWBC. While they found significant changes in the deep properties between occupations, the variability was difficult to characterize and thus challenging to interpret. Here we build on their work and include other nearby sections as well, considering the entire water column. It is reasoned that by using more sections we might objectively extract the dominant interannual trends using an empirical orthogonal function analysis, hopefully leading to a clearer understanding of the variability. By slightly expanding the domain along the boundary, we increased the number of full-depth hydrographic sections to 8 ([Fig. 1](#), solid triangles). These represent all the sections in the historical record extending across the entire slope near this longitude ([Table 1](#)). Since they are not exact repeats, it required special effort to standardize them in order to perform a quantitative analysis (see below).

The second set of sections used in this study is the collection of International Ice Patrol (IIP) exact repeats at 50°W ([Fig. 1](#)). They do not span the same time period as the 55°W sections, nor do they extend to the bottom. These sections were used in order to shed more light on the upper-layer circulation, in particular the slopewater jet and Labrador Current (the latter of which is not sampled by the 55°W sections).

### *a. Standardizing the sections*

Because the 55°W sections were not occupied at precisely the same location, it is not straightforward to compare them quantitatively. To enable such an analysis we employed a coordinate system where bottom depth is the abscissa and depth (or density) the ordinate. In this way each of the sections in its entirety can be plotted on the same grid. This is similar to the approach employed by [Pickart \(1992\)](#) for a collection of sections in the Middle Atlantic Bight. For the deep circulation it is a natural coordinate system, as the flow generally follows the topography.

Each of the 55°W sections was gridded onto two standard coordinate systems—depth versus bottom depth and density versus bottom depth—then carefully scrutinized against the original depth versus distance contour plot ([Fig. 4](#)). Because of the differences in presentation and their associated grid spacings, not every feature is contoured exactly the same in the

three systems. This should not be considered a source of error; after all, contouring is a bit of an art and the same feature may often be contoured numerous ways. In our case we made sure that all major features were represented in consistent fashion in each grid (e.g., consult [Fig. 4](#)). Occasionally this resulted in omitting a closely spaced station. As a check on our procedure, we had the ability to untransform the gridded sections back to distance space and overlay them onto the originals. While this was not done for every variable on every occupation, we did it enough to demonstrate that our approach is indeed successful. For the IIP exact repeat sections at 50°W, we simply gridded the data onto the standard depth versus distance coordinate system.

## *b. EOF analysis*

That all sections are represented on the same grid (vs bottom depth at 55°W and vs distance at 50°W) allows us to compute empirical orthogonal functions in both depth space (EOFs) and density space (DEOFs). It is to be remembered, however, that not every grid point contains all occupations, that is, there is not complete overlap on all sections. Only that part of the domain with at least five realizations at 55°W and nine realizations at 50°W was considered in the EOF analysis. We used the cross-correlation matrix rather than the covariance matrix, because of the difference in the magnitude of the signals between the shallow and deep parts of the water column. In computing the cross-correlation between two grid points, only those realizations corresponding to the same occupations were used (which varied depending on the particular grid points involved). In some ways this can be thought of as a “sparse” EOF calculation, though the consistency and physical nature of the results clearly demonstrate the success of the approach.

Rather than present the results at 55°W in the bottom depth coordinate frame, we computed the average cross-stream bathymetric profile using all the 55°W sections. All output was then transformed back into the cross-stream perspective using this average bathymetry curve. Thus, all results presented in this paper (both 55°W and 50°W) are in the familiar depth versus distance perspective. For the DEOFs, the results are presented in an analogous fashion using the scaled vertical coordinate invoked by PS.

## **4. Upper-layer flow at 55°W: The slopewater current**

### *a. Average properties*

The full water-column average fields at 55°W computed in bottom depth space (then transformed back to distance space) do not differ significantly from the analogous means computed by PS for their subset of the four exact repeats. Hence, we do not show them here [aside from the mean salinity and absolute geostrophic velocity fields from [PS](#) reproduced in [Fig. 3](#)]. However, since the earlier study focused only on the subthermocline flow, we do show the mean distributions for the upper 500 m ([Fig. 5](#)).

The dominant feature, present in all of the individual sections as well, is the presence of a strong front in both temperature and salinity (near 100 km in [Figs. 5a and 5b](#)). This is the slopewater front/jet discussed in [section 2](#). Like the shelfbreak front situated farther onshore (not sampled by our 55°W sections), the slopewater front is a boundary between colder, fresher water to the north and warmer, saltier water to the south. However, there is a fundamental difference between the two fronts in that the isotherms slope upward with offshore distance in the shelfbreak front, while they slope downward with offshore distance in the slopewater front ([Fig. 5](#)). Furthermore, whereas salinity dictates the lateral density gradient in the shelfbreak front (i.e., below the seasonal pycnocline), this is true only down to about 120 m in the slopewater front: deeper than this the temperature variation determines the sense of the density front ([Fig. 5c](#)). This obviously has ramifications regarding the structure of the jet. Another interesting (and apparently ubiquitous) feature of the front is the seaward extension of the near-surface low-salinity layer ([Fig. 5b](#)). Note the corresponding regions of weak lateral salinity gradients (near 150 and 250 km) where this happens. This is apparently tied to the dynamics of the eastward flow as well, as discussed below.

Historical estimates of the transport of the slopewater current south of Newfoundland vary significantly. From the Gulf Stream '60 data, Fuglister (1963) computed transports ranging from 2 to 9 Sv ( $\text{Sv} \equiv 10^6 \text{ m}^3 \text{ s}^{-1}$ ) referenced to 2000 m. Worthington (1976) reported a synoptic estimate of 14.5 Sv also using a deep reference level. Based on a mass balance argument and  $T$ - $S$  considerations, [McLellan \(1957\)](#) estimated a slopewater jet transport between 10 and 20 Sv, fed by two dominant sources. [McLellan \(1957\)](#) argued that about one-quarter of the jet is due to the inflow of Labrador Current Water to the Mid-Atlantic Bight, all of which must eventually recirculate, and the remaining portion originating from the Gulf Stream. All of the above transport estimates are indirect and result from deep reference levels. The mean absolute geostrophic section of [Fig. 3b](#) suggests a much shallower reference level. The slopewater current transport from the individual realizations that make up [Fig. 3b](#) [consult [PS Fig. 11](#)] ranged from .3 to 2.8 Sv. These are on the very low end of the values quoted above.

Using a reference level of 450 m suggested from [Fig. 3b](#) (i.e., the average level of no motion in the region of the jet) we calculated the mean upper-layer thermal wind field from our 55°W sections ([Fig. 5d](#)). As expected, the main

slopewater jet is located near 100 km and has a subsurface maximum, situated at the depth where the lateral temperature and salinity gradients across the front exactly compensate. A more subtle feature of the jet is its seaward “shoulder,” which is surface intensified. Also note the eastward flow at the very offshore end of the section. These two additional jetlike features correspond laterally to where the near-surface freshwater extends offshore as noted above. The transport of the slopewater jet (and shoulder) is 2.1 Sv; adding in the offshore contribution boosts this number by a factor of 2.

## b. Synoptic realization

As mentioned above, the slopewater front was present in each of the individual hydrographic sections. During the occupation of the most recent section (in 1995) we were fortunate to have a vessel-mounted ADCP, which measures horizontal currents as deep as 500 m. In order to help assess the meaningfulness of the mean-referenced thermal wind field (Fig. 5d), as well as consider the instantaneous structure of the slopewater jet, we closely examined the ADCP data from the 1995 section. Five-minute ensembles were collected during the cruise, and we extracted only those profiles corresponding to when the ship was under way (collapsing the shiptrack to the line of best fit through the CTD stations, and interpolating the velocities onto a regular grid).

The vertical section of alongstream ADCP velocity clearly reveals the slopewater jet. Overall, the section is quite similar to the mean thermal wind field (compare Figs. 6a and 5d): The instantaneous jet has a subsurface maximum, precisely where the lateral density gradient vanishes in the corresponding CTD density section (not shown). Additionally, the surface-intensified shoulder of the jet is located seaward of this where the low-salinity near-surface water extends past the main front (Fig. 6b). Both of these features are just as they appear in the mean sections (Fig. 5), adding credence to the structure of the mean jet derived via thermal wind.

As expected, the synoptic realization of the slopewater jet is significantly narrower and stronger than the mean current (maximum speed of  $35 \text{ cm s}^{-1}$  vs  $8 \text{ cm s}^{-1}$ ). The surface front in the shipboard thermosalinograph record (not shown) corresponds nicely to the ADCP velocity jet; as with the Gulf Stream, the surface property front is located slightly shoreward of the subsurface velocity core. Note that the ADCP data do not extend deep enough to determine definitively the reference level, though there is the suggestion that such a level might exist near 500 m, consistent with Fig. 3b. (If the 1995 thermal wind section is referenced using the shipboard ADCP data, the corresponding level of no motion occurs at 550 m.) The transport of the instantaneous jet (including the shoulder) is 3.3 Sv, a bit larger than but comparable to the mean value.

The evidence presented here thus suggests that the transport of the slopewater current (not including the eastward flow at the offshore edge of our domain) is on the order of 2–3 Sv, considerably less than most of the historical values. This is due to the shallow reference level revealed by the absolute measurements, in contrast to the deeper reference levels chosen subjectively by previous authors.

## c. Variability

Performing a shallow (0–800 m) EOF analysis on the set of 55°W CTD sections reveals a dominant mode of variability of the slopewater front. The temperature and salinity EOF vertical structure fields show the entire domain becoming cooler and fresher (or warmer and saltier), with maximum amplitude at the surface near the mean position of the front (Fig. 7). This is reminiscent of Gulf Stream variability and suggests simple lateral translation of the front. To document that this is so, we tabulated the frontal location in each of the sections and compared it to the EOF modal amplitude (Fig. 8). The agreement clearly indicates that this is the correct physical interpretation of the mode (which contains three times the variance of the next dominant mode).

Note the difference between the temperature and salinity EOF structure fields at the seaward end of the domain: the region of high salinity variance extends much farther offshore in the near-surface layer. This feature is strong enough to impact the associated density EOF such that its vertical structure does not have the same sign throughout the domain (as did  $T$  and  $S$ , Fig. 7). To help visualize what this means, we added the EOF fields back into the mean and compared the minimum and maximum realizations (Fig. 9). The first thing to note is that the mode does indeed correspond to lateral translation of the slopewater front as expected. However, when the front moves offshore, the low-salinity surface water extends much farther seaward relative to the frontal location. This freshwater in turn leads to a light near-surface layer that is not otherwise present (i.e., the manifestation of the aforementioned EOF structure). The conclusion is that when the front moves southward, the low-salinity surface slopewater is able to progress significantly beyond the main front.


Using the 450-m reference level, we computed the geostrophic velocity of the mode (Fig. 9). The current (both the subsurface jet and surface-intensified shoulder) is significantly stronger when onshore due to the steepening of the density front. Its transport increases from 2.1 Sv (offshore) to 4.0 Sv (onshore). Curiously, only when the front is offshore does the region of eastward flow appear at the seaward edge of the section (which was seen in the mean field, Fig. 5d). As pointed out above, this feature has significant transport, so even though the jet is stronger when onshore, the total eastward

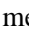
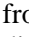
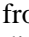
transport through the section is greater when the jet is offshore (6.3 Sv).

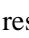
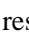

Many questions arise from our simple analysis. What is the nature of the jet's lateral movement? Is it a continuous jet that "meanders," and if so on what timescales? How is the jet impacted by the Gulf Stream to the south and shelfbreak current to the north? What is its fate farther east? While many such issues await further study, below we shed some light on the nature of the jet's variability and its relationship to other components of the slopewater circulation.

## 5. Upper-layer flow at 50°W: Shelfbreak and slope

### a. Average properties


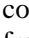
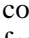
As discussed in the overview, the slopewater current extends eastward at least as far as 50°W, as revealed by the IIP sections at that longitude ([McLellan 1957](#)). The IIP data consist of a set of standard hydrographic sections occupied in the region between the Grand Banks of Newfoundland and Flemish Cap between 1948 and 1978. Both the duration of the program and the regularity of the sampling pattern were remarkable and offer a great opportunity to study interannual variability in the region. The major caveat is that the sections were only occupied during the months of April, May, and June (iceberg season). Since there have been few quantitative studies addressing the variability in the IIP data and because our sections at 55°W did not extend to the shelfbreak, we decided to analyze the 50°W IIP sections in a manner akin to the 55°W sections. Our hope was not only to quantify the slopewater jet at this location but to investigate its relationship to the Labrador Current, which flows westward along the shelfbreak. Here we analyze the time period from 1949 to 1963 ([Fig. 1](#) , which are all bottle measurements) and consider the April sections only in order to avoid a seasonal signal.

Most of the 50°W sections extended far enough offshore to measure the slopewater front, which shows up clearly in the mean sections ([Fig. 10](#) ). It would have been useful had stations regularly been occupied a bit farther south, though apparently the detection of the front was used as a criterion for ending the section. In any case, the main portion of the front is clearly resolved in the dataset. Note the presence of the westward-flowing Labrador Current as the cold, fresh water mass banked against the shelfbreak. As is true of the shelfbreak current farther west (e.g., [Linder and Gawarkiewicz 1998](#)), the density change across this front is everywhere determined by the salinity (i.e., lighter water inshore of denser water). The relationship between the Labrador Current and the slopewater jet is one of the things we wish to consider. Inspection of the mean fields reveal some significant differences between the slopewater front at this longitude versus that at 55°W. Here the front is stronger and extends deeper (cf. [Figs. 5a](#)  and [10a](#) ). Note also that the temperature variation across the front dictates the sense of the density change starting at a much shallower depth (i.e., the reversal of the density front occurs near 15 m at 50°W vs 120 m at 55°W). Thus, the structure of the front at 50°W is more akin to that of the Gulf Stream.

The increased strength of the mean front implies a larger baroclinic transport. To be consistent with the 55°W sections we referenced the IIP thermal wind velocities to 450 m as well (except near the shelfbreak where we used the bottom). It should be stressed, however, that unlike 55°W there is no compelling reason for this choice. The mean slopewater flow referenced as such is 6.4 Sv, which is three times larger than the jet farther upstream. However, adding in the eastward flow at the offshore edge of the mean 55°W section makes the two values more comparable (also bear in mind that we do not resolve the total eastward flow of slopewater at either location, [Figs. 5d](#)  and [10d](#) ). It is worth mentioning that the Gulf Stream converges toward the boundary near the Grand Banks ([Fig. 2](#) , thereby shrinking the lateral extent of the slopewater region. It is thus possible that in the west, where the domain is considerably wider, the eastward slopewater flow occurs in multiple bands, which then merge to form a single, more intense jet at 50°W—while conserving the total transport. Of course it is also possible that the total transport is simply greater near the Grand Banks. Further measurements are needed to sort this out definitively. The westward transport of the Labrador Current in the mean 50°W section is 2.5 Sv, comparable to the value quoted by [McLellan \(1957\)](#).

### b. Variability

Unlike the upper layer at 55°W, the variability in the 50°W sections is not dominated by a single EOF mode—despite the apparent presence of the same slopewater jet. Rather, the variability is more complex near the Grand Banks (note also that by resolving the Labrador Current another degree of freedom is added to the system). We discuss the first two modes because they have a clear physical interpretation and their associated variability is readily apparent in the original sections.<sup>2</sup>

The first mode corresponds to strengthening/weakening of the slopewater front ([Fig. 11](#) ). Note the structure of the corresponding theta mode versus that at 55°W (cf. [Fig. 11a](#)  vs [7a](#) ). Here the zero-line runs through the center of the front (i.e., when the front strengthens the inshore side cools while the offshore side warms). Mode 2 (not shown) is associated with lateral translation of the front, which was the dominant mode at 55°W. We compared the respective IIP EOF modal amplitudes to the time series of frontal strength and position calculated from the original sections, and again the agreement verified these interpretations. We have no clear idea why the strength of the front varies so much at 50°W compared to 55°W; perhaps it is related to the front's proximity to the Gulf Stream near the Grand Banks.

The variation of the Labrador Current described by these two modes is also significant. In mode 1, when slopewater front is stronger, the Labrador Current is colder and fresher (Fig. 11); this is perhaps intuitive based on the close proximity of the two currents in this region. Note, however, that because salinity has the dominant effect on density in the Labrador Current, the density decreases on the inshore side of the shelfbreak front while simultaneously decreasing on the offshore side of the slopewater front (Fig. 11c). Hence both density fronts steepen. In mode 2 the variation of the Labrador Current is less intuitive. One might envision that, when the slopewater front moves toward the boundary, the water onshore would become uniformly warmer. This is true everywhere except in the Labrador Current, which in fact becomes colder (and fresher). This, together with the fact that the slopewater front sharpens somewhat as it moves onshore, implies that the two density fronts also vary in phase for mode 2.

Thus, both EOF modes result in the simultaneous strengthening/weakening of the shelfbreak current and slopewater jet. Since these two currents respectively represent import and export to the slopewater region (McLellan 1957), the dominant interannual variability revealed in the IIP data suggests a spinup/down of the entire upper-layer slopewater system. To assess the potential magnitude of the change, we computed the hydrographic fields and baroclinic transport of the combined mode 1 + 2 (Fig. 12). In the strengthened state (minimum modal amplitude) the Labrador Current is more than 3°C colder and 0.8 psu fresher, while the slopewater front is strongly enhanced and extends significantly deeper. The geostrophic transports of the two currents are larger by roughly a factor of 4 (Fig. 12). This tendency of the Labrador Current to advect colder water when its transport is enhanced is opposite of that reported by Petrie and Drinkwater (1993), using a portion of the same IIP data. To verify that our result is robust we computed the Labrador Current transport and core temperature using the original sections (i.e., not the EOF modes), and the relationship is readily apparent. It also is intuitive in that a colder/fresher Labrador current implies a stronger density front (dictated by the salinity), hence larger baroclinic transport. It should be noted that the temperatures quoted by Petrie and Drinkwater (1993) were spatially averaged values, and they considered a strongly low-passed temporal signal in transport.

Variability of the Labrador Current water emanating from the subpolar North Atlantic has been investigated at some length, and the associated impacts can be huge. For instance, during the late nineteenth century a catastrophic kill of bottom-dwelling tilefish occurred along the Canadian and U.S. eastern seabords (Collins 1884). This is believed to have been caused by the Labrador Current transporting anomalously large amounts of cold water equatorward of the Grand Banks, apparently related to the extreme minimum state of the North Atlantic Oscillation during that time period (ICES 1995; Marsh 1999, submitted to *Fish Oceanogr.*). Indeed, Myers et al. (1989) note a correlation (albeit weak) between the NAO index and baroclinic transport of the Labrador Current farther north in the Newfoundland basin, such that weaker values of the NAO are associated with larger transports.


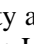
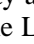

We investigated the relationship of the NAO to the variability observed in the IIP 50°W data. During our period of observation (1949–63) the NAO underwent large interannual oscillations, with the low-passed trend being one of decreasing NAO index (Fig. 13c). Over this period there is no statistically significant correlation between the NAO and either of the IIP EOF modes. This perhaps is not surprising, since it is unclear as to the mechanisms and timescales by which the NAO might impact the structure and transport of the slopewater system west of the Grand Banks. While there seems to be some evidence that a low NAO state favors a stronger, colder Labrador Current (ICES 1995; Myers et al. 1989), the relationship is not a simple one.

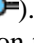
## 6. Coupled shallow–deep variability

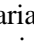

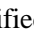
We return now to the 55°W sections and consider the entire water column. (Note that this is impossible to do with the 50°W data because they only extend to 1500 m.) As discussed in the overview the two major subthermocline water masses in the slopewater are the Labrador Sea water (LSW) and Denmark Strait overflow water (DSOW), both of which progress equatorward in the DWBC (Fig. 3b). The mean structure of these components is presented in PS and therefore not elaborated on here, other than to note the mean velocity and salinity fields in Fig. 3. Pickart and Smethie (1998) also addressed the variability of these two water masses using four of the eight sections considered here. Differencing on density surfaces, they showed that the largest fluctuations corresponded to a cooling/freshening of the LSW layer from the 1980s into the 1990s. We computed the full-water column empirical modes in density space using all eight sections (these are referred to as DEOFs).

Not surprisingly, the dominant DEOF shows an extremum in the LSW layer (1500–2000 m, Fig. 13) with the strongest cooling in 1991. This is consistent with Pickart and Smethie's results. However, note the similarity between the amplitude time series of the DEOF and that of the shallow depth space EOF at this location (cf. Figs. 7d and 13b). Note as well the similar spatial structure in the shallow layer of the DEOF. This implies that the cooling/freshening of the LSW layer coincides with the slopewater jet being positioned farther offshore. This is somewhat surprising and suggests that the slopewater jet varies pronouncedly on interannual timescales.<sup>3</sup> The other implication, of course, is that the slopewater jet must not meander in the sense akin to the Gulf Stream, otherwise the resulting mesoscale signal would likely alias any longer-term fluctuations. Instead it may be that any such high-frequency meandering of the slopewater jet is simply on smaller lateral scales than the interannual changes in the jet's position. To further verify the shallow–deep coupling we

computed the DEOF modes of the deep water only; again the amplitude time series is clearly correlated to the shallow water variability.

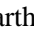
This full water column mode has a clear signal in depth space as well (in fact, it explains nearly 50% of the variance, compared to only 35% in density space). The depth structure of the mode is nicely visualized by comparing the minimum and maximum realizations for potential temperature. The minimum modal state, in which LSW is less prevalent, shows a strong slopewater front positioned onshore (Fig. 14a , left panel). By contrast, the maximum state, with an abundance of LSW (seen by the spreading of the 3° and 4°C isotherms), has the slopewater front farther offshore and weaker (Fig. 14a , right panel). This is consistent with the variability at 50°W, where the front is also weaker when it resides offshore (Fig. 12 ). In addition to the widening and cooling of the LSW layer in the maximum modal state, the corresponding oxygen mode shows significantly higher tracer concentrations (hence stronger ventilation) in the LSW during these periods (Fig. 14b 

Pickart and Smethie also discussed the relationship between the variation of LSW and that of the deeper DSOW; however, the nature of the relationship remained a puzzle. Using our EOF modes we are in a better position to address this issue. In the minimum modal state the potential temperature fields indicate that the thermal shear of the DSOW is stronger (e.g., note the increased slope of the 2°C isotherm in Fig. 14a ). Such a strengthening of the deep flow is completely opposite of the notion put forth by PS who based their view largely on the single section occupied in 1991. To investigate this carefully, we focused on the DSOW and computed the corresponding depth EOFs of the deep layer only.

The dominant deep density mode nicely shows the enhancement of the DSOW shear during the minimum state (Fig. 15 ). Although this mode explains only 34% of the variance, it clearly corresponds to the oxygen mode: In the minimum state the DSOW oxygen core is located downslope, coincident with the region of large thermal wind shear (near  $x = 135$  km, Fig. 15a x = 100 km, Fig. 15b 

Part of the reason for the reduced variance explained by the dominant deep density mode, compared to oxygen, is due to the 1991 section. This section has a strong deep thermal signal that appears mainly in mode 2 (not shown), which can be interpreted as a pure strengthening/weakening mode (i.e., the DWBC pulses but does not move—clearly distinct from the coupled mode described above). This probably explains why PS had difficulty putting the 1991 DSOW signal into context with their other results. Indeed, the deep velocity signal in 1991 is anomalous, which highlights the danger of using small numbers of repeat sections to deduce climate-type variability. Pickart and Smethie (1998) used four repeat sections; it was not until an EOF calculation was done using twice that number of sections that the clear coupled signal emerged.

It does, of course, remain to be determined how the strength of the middepth LSW circulation varies in the coupled mode. Both the near-surface and near-bottom flow along the western boundary spins up in the minimum state, but we were able to determine this definitively because both of these components have a large baroclinic signal. Clearly, the LSW property signal diminishes in this state, so one is tempted to conclude that the flow might diminish. However, based on the enhanced circulation both above and below, this cannot be taken as obvious.

It is tempting to think of the coupled slopewater mode as an “NAO” mode, with the minimum modal state corresponding to a low NAO, and vice versa. Enhanced air–sea buoyancy forcing over the Labrador Sea during high NAO years has been linked to increased production of LSW (e.g., Dickson et al. 1997), which in turn leads to more undiluted LSW downstream in the DWBC (Pickart et al. 1997). Our maximum modal state includes a prevalence of such LSW in the boundary current. Note that the low-passed NAO increased substantially from the 1980s to the 1990s (Fig. 13c 

## 7. Conclusions

Using two sets of repeat hydrographic sections centered at 55°W and 50°W, we have elucidated some of the mean features of the slopewater current system south of Newfoundland and identified an intriguing coupled mode of variability.

In the upper portion of the water column, the slopewater current transports water eastward inshore of the Gulf Stream. While previous studies have documented the existence of this current, we have presented the most quantitative view to date of the jet's structure and transport. Strong fronts exist in both temperature and salinity that compensate each other to



differing extent over the top 500 m. At 55°W the salinity determines the sense of the density front down to 125 m, while below temperature has the dominant effect. This results in a subsurface jet with a surface-intensified “shoulder,” transporting 2–3 Sv in the mean. This is significantly less than previous estimates (all of which were indirectly referenced). At 50°W the slopewater front is stronger and extends deeper; correspondingly the mean transport is larger (three times larger using the same reference level as 55°W). The nature of the jet’s continuity between the two longitudes remains to be investigated. Inshore of the jet resides the westward-flowing Labrador Current banked against the shelfbreak. Its mean transport at 50°W is 2.5 Sv (referenced to the bottom), in line with previous estimates.

An EOF analysis of the 55°W sections shows that the entire water column varies in coupled fashion on interannual timescales. While this was expected for the deeper water mass components of the DWBC based on earlier work, the covariation of the slopewater jet was a surprise. This coupled slopewater mode is illustrated schematically in [Fig. 16](#). During the “minimum” modal state, when the LSW is less well ventilated, the slopewater jet is stronger and located onshore. At the same time the DSOW component of the DWBC strengthens. By contrast in the “maximum” modal state—when there is a prevalence of newly ventilated LSW at middepth—both the upper-layer slopewater jet and bottommost DWBC weaken, and the slopewater jet moves offshore.

At 50°W the upper-layer variability is more complex, yet largely consistent with that farther to the west. Both the strength and position of the slopewater jet at this longitude are coupled to variations of the Labrador Current. The overall suggestion from the two sets of sections ([Fig. 16](#)) is that the entire upper-layer slopewater system spins up (down) on interannual timescales, in phase with strengthening (weakening) of the deepest DWBC flow. How and if these water-column-wide fluctuations are tied to the NAO cycle remains to be determined.

### Acknowledgments

This project was supported under National Science Foundation Grant OCE-9301448 and Office of Naval Research Contract N00014-95-1-0575. Comments from two anonymous reviewers resulted in substantial improvement in the presentation of the work.

---

## REFERENCES

- Bacon, S., 1998: Decadal variability in the outflow from the Nordic Seas to the deep Atlantic Ocean. *Nature*, **394**, 871–874.
- Clarke, R. A., H. W. Hill, R. F. Reiniger, and B. A. Warren, 1980: Current system south and east of the Grand Banks of Newfoundland. *J. Phys. Oceanogr.*, **10**, 25–65. [Find this article online](#)
- Collins, J. W., 1884: History of the tilefish. U.S. Commn. on Fish and Fisheries, Rep. Commissioner V(1882), 237–294.
- Csanady, G. T., and P. Hamilton, 1988: Circulation of slopewater. *Contin. Shelf Res.*, **8**, 565–624.
- Curry, R. G., M. S. McCartney, and T. M. Joyce, 1998: Oceanic transport of subpolar climate signals to middepth subtropical waters. *Nature*, **391**, 575–577.
- Dickson, R. R., J. R. N. Lazier, J. Meincke, P. B. Rhines, and J. Swift, 1996: Long-term coordinated changes in the convective activity of the North Atlantic. *Progress in Oceanography*, Vol. 38, Pergamon, 241–295.
- Fofonoff, N. P., and M. M. Hall, 1983: Estimates of mass, momentum, and kinetic energy fluxes of the Gulf Stream. *J. Phys. Oceanogr.*, **13**, 1868–1877. [Find this article online](#)
- Fuglister, F. C., 1963: Gulf Stream ‘60. *Progress in Oceanography*, Vol. 1, Pergamon, 265–383.
- , and L. V. Worthington, 1951: Some results of a multiple ship survey of the Gulf Stream. *Tellus*, **3**, 1–14.
- Hendry, R., 1993: Currents south of the Grand Banks at 50W: Estimates of mass transport. *The North Atlantic Current System: A Scientific Report*, Rizzoli and T. Rossby, Eds., 132 pp.
- ICES, 1995: Report of the Cod and Climate Backward-Facing Workshop. Bedford Institute of Oceanography, Dartmouth, NS, Canada, 8-ICES, 23 pp.
- Lazier, J. R. N., and D. G. Wright, 1993: Annual velocity variations in the Labrador Current. *J. Phys. Oceanogr.*, **23**, 559–678. [Find this article online](#)
- Linder, C. A., and G. G. Gawarkiewicz, 1998: A climatology of the Shelfbreak Front in the Middle Atlantic Bight. *J. Geophys. Res.*, **103**,

Loder, J. W., B. Petrie, and G. Gawarkiewicz, 1998: The coastal ocean off northeastern North America: A large-scale view. *The Sea, Coastal Segment I*, A. Robinson and K. Brink, Eds., Vol. 11, 105–133..

Mann, C. R., 1967: The termination of the Gulf Stream and the beginning of the North Atlantic Current. *Deep-Sea Res.*, **14**, 337–359..

McLellan, H. J., 1957: On the distinctness and origin of the slope water off the Scotian shelf and its easterly flow south of the Grand Banks. *Fish. Res. Bd. Canada*, **14**, 213–239..

Mountain, D. G., and J. L. Shuhy, 1980: Circulation near the Newfoundland Ridge. *J. Mar. Res.*, **38**, 205–213..

Myers, R. A., J. Helbig, and D. Holland, 1989: Seasonal variability of the Labrador Current and West Greenland Current. Paper C.M. 1989/c:16, ICES, 10 pp..

Petrie, B., and K. Drinkwater, 1993: Temperature and salinity variability on the Scotian Shelf and in the Gulf of Maine 1945–1990. *J. Geophys. Res.*, **98**, 20 079–20 089..

Pickart, R. S., 1992: Space–time variability of the deep western boundary current oxygen core. *J. Phys. Oceanogr.*, **22**, 1047–1061.. [Find this article online](#)

—, and W. M. Smethie Jr., 1993: How does the deep western boundary current cross the Gulf Stream? *J. Phys. Oceanogr.*, **23**, 2602–2616.. [Find this article online](#)

—, and R. X. Huang, 1995: Structure of an inertial deep western boundary current. *J. Mar. Res.*, **53**, 739–770..

—, and —, 1998: Temporal evolution of the Deep Western Boundary Current where it enters the sub-tropical domain. *Deep-Sea Res.*, **45**, 1053–1083..

—, M. A. Spall, and J. R. N. Lazier, 1997: Mid-depth ventilation in the western boundary current system of the sub-polar gyre. *Deep-Sea Res.*, **44**, 1025–1054..

Richardson, P. L., 1985: Average velocity and transport of the Gulf Stream near 55W. *J. Mar. Res.*, **43**, 83–111..

Worthington, L. V., 1976: *On the North Atlantic Circulation*. The Johns Hopkins Oceanographic Studies, No. 6, 110 pp..

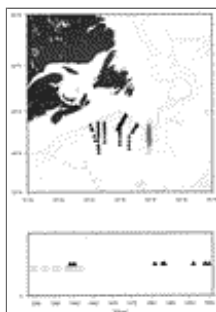
## Tables

Table 1. 55°W Hydrographic sections.


Ship	Cruise	Stations	Dates of section	Year	Type
<i>Crawford</i>	28	17–23	06/22–06/24	1959	Water sample
<i>Crawford</i>	40	42–51	04/20–04/22	1960	Water sample
<i>Oceanus</i>	134	58–67	07/03–07/06	1983	CTD
<i>Knorr</i>	89	243–249	10/14–10/16	1981	CTD
<i>Oceanus</i>	133	291–301	05/16–05/17	1983	CTD
<i>Endeavor</i>	223	2–10	03/28–03/30	1991	CTD
<i>Endeavor</i>	257	2–9	11/11–11/14	1994	CTD
<i>Oceanus</i>	269	2–10	05/30–06/10	1995	CTD

[Click on thumbnail for full-sized image.](#)

## Figures



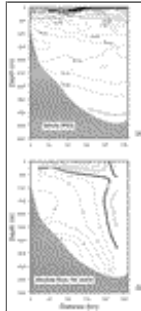
[Click on thumbnail for full-sized image.](#)

Fig. 1. Hydrographic sections used in the analysis. Upper panel: The black triangles are full-water column stations clustered around 55°W, and the open gray circles are the International Ice Patrol stations at 50°W, which extend only to 1500 db. The bathymetric contours are 1000–4000 m. Lower panel: Temporal distribution of the data (see also [Table 1](#) )



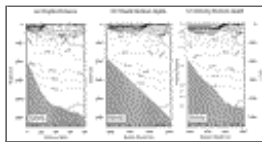
[Click on thumbnail for full-sized image.](#)

Fig. 2. Schematic circulation in the region of the Grand Banks of Newfoundland. Black lines are the upper-layer currents and gray lines represent the deep flow. Question marks signify areas of possible interactions. The bathymetric contours are 200 m, 1000–5000 m.



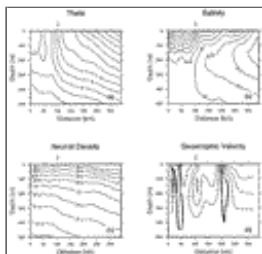
[Click on thumbnail for full-sized image.](#)

Fig. 3. Mean salinity and absolute geostrophic velocity at 55°W from PS (using a subset of the 55°W sections used in the present study). The geostrophic velocity section was referenced using acoustic transport floats; see PS for details.



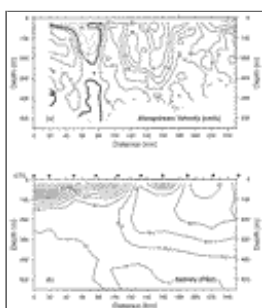
[Click on thumbnail for full-sized image.](#)

Fig. 4. Vertical section of salinity (*Oceanus* cruise 134, 1983) gridded onto the three coordinate systems. The EOF analyses were done using the two bottom-depth systems.



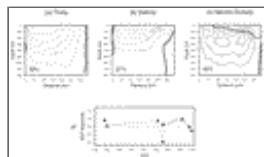
[Click on thumbnail for full-sized image.](#)

Fig. 5. Mean sections in the depth range 0–500 m (in depth space) at 55°W. Variables plotted are theta (°C), salinity (psu), neutral density, and geostrophic velocity (cm s<sup>-1</sup>). The arrow marks the position of the slope water front/jet.



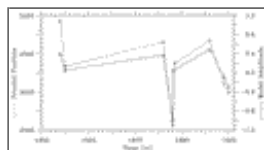
[Click on thumbnail for full-sized image.](#)

Fig. 6. (a) Shipboard ADCP section of alongstream velocity (59°T) at 55°W collected in 1995. (b) CTD section of salinity occupied at the same time (inverted triangles denote the station positions).



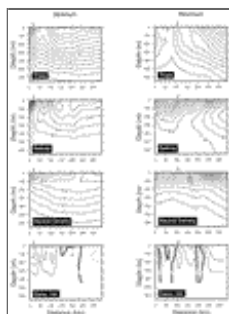
Click on thumbnail for full-sized image.

Fig. 7. Dominant EOF mode in the upper 800 m (depth space) at 55°W. The amplitude time series is the average for the three variables, where the standard deviation is denoted by the gray shading. The percent variance explained by the mode is indicated for each variable. The dimensional value of the mode is obtained by multiplying the amplitude time series by the vertical structure fields. (Note: for all of the EOF plots, the amplitude time series has been normalized to a maximum value of 1, thus the value of the vertical structure fields may be interpreted as the maximum dimensional value of the mode.)



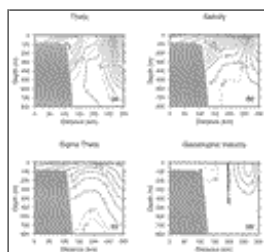
Click on thumbnail for full-sized image.

Fig. 8. Comparison of the EOF modal amplitude from [Fig. 7](#) to the lateral position of the slopewater front.



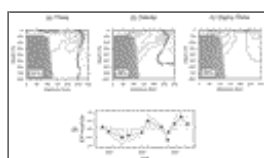
Click on thumbnail for full-sized image.

Fig. 9. Minimum and maximum values of the EOF mode from [Fig. 7](#) added back into the mean (allowing the reader to visualize the physical significance of the mode). The arrow denotes the location of the slopewater front/jet.



Click on thumbnail for full-sized image.

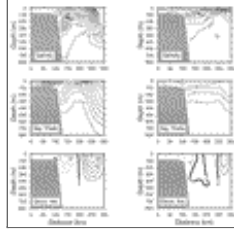
Fig. 10. Mean sections in the depth range 0–800 m (in depth space) at 50°W. Variables plotted are theta (°C), salinity (psu), potential density ( $\text{kg m}^{-3}$ ), and geostrophic velocity ( $\text{cm s}^{-1}$ ).




Click on thumbnail for full-sized image.

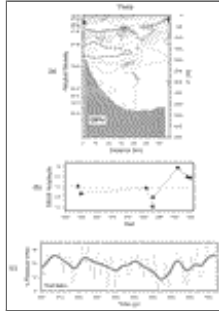
Fig. 11. Dominant EOF mode in the upper 800 m (depth space) at 50°W (presented as in [Fig. 7](#)).





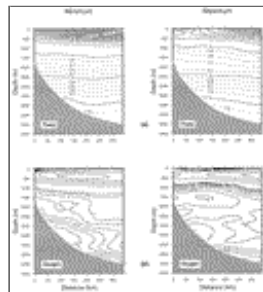
Click on thumbnail for full-sized image.

Fig. 12. Minimum and maximum values of the combined EOF mode 1 + 2 at 50°W (presented as in [Fig. 9](#) .



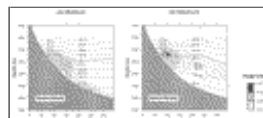
Click on thumbnail for full-sized image.

Fig. 13. Dominant full water-column theta DEOF mode (density space) at 55°W. The section is plotted using scaled depth (see PS), with the values of neutral density shown as well. (a) Vertical structure of mode (the contour that delimits the middepth LSW extremum is bold). (b) Amplitude time series of mode. (c) Time series of the North Atlantic oscillation index, which is the winter sea level pressure difference between Iceland and the Azores. The dotted line marks the yearly values, and the thick line is the 12-yr low pass.



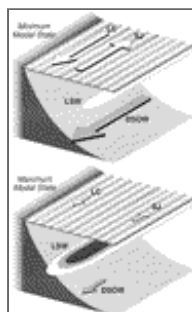
Click on thumbnail for full-sized image.

Fig. 14. Minimum and maximum values of the dominant full water-column EOF mode (depth space) at 55°W: Theta (°C) and oxygen ( $\text{ml l}^{-1}$ ).



Click on thumbnail for full-sized image.

Fig. 15. Minimum and maximum values of the dominant deep water EOF mode (depth space) at 55°W: Neutral density (contours) overlaid by oxygen (shading).



Click on thumbnail for full-sized image.

Fig. 16. Schematic depicting the two states of the coupled slopewater EOF mode in which LC: Labrador Current, SJ: slopewater

<sup>1</sup> Warm core rings may also be responsible for synoptic measurements of counterflow.

<sup>2</sup> The 1951 and 1954 sections were excluded from the analysis. In both cases there was an unusually large amount of warm water far onshore that dominated the EOF calculation. This may be due to the Gulf Stream being anomalously far north, as it was for instance in the 1972 50°W section of [Clarke et al. \(1980\)](#). However, the IIP sections do not extend far enough offshore to determine if this is the cause.

<sup>3</sup> Worthington's (1964) paper entitled "Anomalous conditions in the slope water area in 1959" discussed a cooling of the deep waters associated with an offshore displacement of the slopewater front. He contrasted the conditions in 1959 to those observed one year later in 1960 (both occupations are included in our collection of 55°W sections). Our EOF analysis demonstrates that 1959 was, in fact, not anomalous but simply part of this interannual mode.

\* WHOI Contribution Number 9595.

*Corresponding author address:* Dr. Robert S. Pickart, Woods Hole Oceanographic Institution, Woods Hole, MA 02543.

E-mail: [rpickart@whoi.edu](mailto:rpickart@whoi.edu)

top ▲



© 2008 American Meteorological Society [Privacy Policy and Disclaimer](#)  
Headquarters: 45 Beacon Street Boston, MA 02108-3693  
DC Office: 1120 G Street, NW, Suite 800 Washington DC, 20005-3826  
[amsinfo@ametsoc.org](mailto:amsinfo@ametsoc.org) Phone: 617-227-2425 Fax: 617-742-8718  
[Allen Press, Inc.](#) assists in the online publication of *AMS* journals.